Journal of
Materials Chemistry A

Materials for energy and sustainability

Accepted Manuscript

This article can be cited before page numbers have been issued, to do this please use: D. Kim, J. Jang, J. Jung, J. Ku, Y. S. . Park, J. Lee and A. Lee, *J. Mater. Chem. A*, 2026, DOI: 10.1039/D6TA02924H.

ROYAL SOCIETY OF CHEMISTRY

rsc.li/materials-a

View Article Online
DOI: 10.1039/D6TA02924H

ARTICLE

Effect of Terphenyl Isomeric Structure on Poly(diallyldialkylammonium)-Functionalized Anion Exchange Membranes for Water Electrolysis

Received 00th January 20xx,
Accepted 00th January 20xx

DOI: 10.1039/x0xx00000x

Dana Kim[a,b], Jeongmin Jang[a], Jiyoon Jung[a], Jinsuk Ku[c], Young Sang Park[a], Jung-Hyun Lee*[b] and Albert S. Lee*[a,c]

The structural design of anion exchange membranes (AEMs) critically affects their ionic conductivity, mechanical strength, and alkaline stability—key requirements for high-performance AEM water electrolyzers (AEMWEs). Herein, we report a backbone isomerism engineering strategy to modulate hydration and transport properties by synthesizing m-terphenyl and p-terphenyl units as rigid aromatic backbones, functionalized with pyrrolidinium groups via cyclopolymerization and covalent crosslinking. Beyond homopolymer studies, physical blends, and random copolymers were systematically compared to investigate how backbone geometry and integration method influence membrane properties. All membranes exhibited low swelling and relatively high mechanical strength under wet conditions, while hydration and conductivity varied depending on structure and polymer type. m-Terphenyl-based AEMs formed a twisted, microporous structure, providing higher free volume, water uptake, and hydroxide conductivity than their p-terphenyl counterparts. In contrast, p-terphenyl-based membranes exhibited superior mechanical strength and alkaline stability due to their linear conformation. Blends and copolymers showed intermediate properties, balancing hydration and mechanical robustness. Incorporating water electrolysis performance and durability, these structural variations were found to directly influence practical AEMWE operation. Notably, the m-terphenyl-based membrane achieved high AEMWE performance of 8.6 A/cm² at 2.0 V using non-platinum group metal anode, outperforming the blend, copolymer, and p-terphenyl-based membranes. This study provides the first comprehensive correlation between terphenyl isomerism and AEM performance, offering molecular-level insights into how backbone architecture can be tailored to enhance electrochemical functionality.

1. Introduction

Green hydrogen production through anion exchange membrane water electrolyzers (AEMWEs) is promising for cost-effective energy due to non-platinum catalysts and mild alkaline conditions.[1-4] However, anion exchange membranes (AEMs) face challenges like low ionic conductivity—hydroxide ions move slower than protons—leading to higher resistance and energy use.[5,6] They also suffer from limited alkaline/mechanical stability, causing shorter lifetimes (~2,000 h) compared to proton exchange membrane water electrolyzers (PEMWEs).[7] Degradation of polymer backbones and quaternary ammonium groups results in brittleness and breakdown in alkaline environments.[8] Increasing water uptake boosts conductivity but causes swelling and instability, reducing durability.[9,10] To address this, aryl ether-free polymers like poly(phenylene)s with rigid backbones are used for better chemical stability.[11,12] Cyclic quaternary ammoniums such as pyrrolidinium improve alkaline resistance by avoiding elimination-prone hydrogens,[8,13] and crosslinking enhances mechanical strength and limits swelling.[14]

In the early development of AEMs, tetramethylammonium (TMA) was commonly used as a cation, but its limited alkaline stability led to the exploration of more stable alternatives.[15] Recent studies have shown that cyclic ammoniums like dimethyl piperidinium (DMP) and 6-azonia-spiro[5.5]undecane (ASU) offer improved stability compared to TMA, while 5-membered ring compounds like dimethyl pyrrolidinium (DMPy) exhibit reduced stability due to ring strain. In fact, the alkaline stability of these quaternary ammonium groups in 6 M NaOH at 160°C showed half-lives of 61.9 hours for TMA, 87.3 hours for DMP, 110 hours for ASU, and 37.1 hours for DMPy.[13] Although various studies have demonstrated that pyrrolidinium rings are generally susceptible to degradation in alkaline environments, several works have reported that they can exhibit satisfactory alkaline stability under certain conditions. Xu et al. investigated the effects of piperidinium and pyrrolidinium cation structures on AEM properties, including alkaline stability, using styrene-b-ethylene-b-butylene-b-styrene (SEBS) as the backbone polymer.[16] After immersing the membranes in 1M KOH at 90 °C for over 700 hours, both piperidinium-based and pyrrolidinium-based membrane maintained approximately 95 % of their initial conductivity. This result indicates that pyrrolidinium-based

[a] Extreme Materials Research Center, Korea Institute of Science and Technology (KIST), Seoul 02792, Republic of Korea.
[b] Department of Chemical and Biological Engineering, Korea University, Seoul 02841, Republic of Korea. E-mail: leejhyyy@korea.ac.kr
[c] Convergence Research Center for Solutions to Electromagnetic Interference in Future-Mobility, Korea Institute of Science and Technology (KIST), Seoul 02792, Republic of Korea. E-mail: aslee@kist.re.kr
* Corresponding authors.

AEMs exhibit similar chemical stability to those with piperidinium, demonstrating that pyrrolidinium cations also maintain good alkaline stability under prolonged exposure. Gjoshi et al. evaluated the stability of AEMs based on piperidinium and pyrrolidinium groups.[17] They introduced piperidinium and pyrrolidinium cations into a poly(oxindole biphenyl-co-trifluoroacetophenone) backbone via a long pentyl chain. The synthesized AEMs were immersed in 2 M aqueous KOH at 80 °C for one month. After two weeks, no new NMR peaks were observed for the pyrrolidinium-based membrane, whereas the piperidinium-based membrane exhibited peaks corresponding to vinylic protons resulting from ring-opening Hofmann β-elimination.

Recent studies have emphasized the critical role of polymer backbone geometry and intrinsic free volume in enhancing AEM performance. Increased free volume facilitates water uptake and hydroxide conductivity by improving hydration and ion transport pathways. For example, Xue et al. reported on the branched architecture–induced effects on free volume and chain entanglement. They prepared anion exchange membranes based on poly(p-terphenyl dimethylpiperidinium) with 1,3,5-triphenylbenzene (TPB) as the branching unit. The branched membranes showed an increased free volume compared to poly(p-terphenyl dimethylpiperidinium) membranes without the branching unit.[18] Also, membranes prepared by increasing the TPB content from 0.5 % to 0.1 % exhibited a higher degree of branching, which led to an increase in free volume and a corresponding increase in water uptake. They also showed enhanced chain entanglement, which provided better mechanical stability.

In parallel, the spatial arrangement of backbone units has been shown to influence membrane properties. Lee et al. investigated the effects of two terphenyl isomers (m-terphenyl and p-terphenyl) incorporated into polymer backbones. They found that m-terphenyl-based membrane exhibit increased free volume and higher ionic conductivity, whereas p-terphenyl-based membrane show enhanced mechanical stability.[19] Gao et al. further compared AEMs incorporating three terphenyl isomers (o-, m-, and p-), identifying p-terphenyl as providing the best balance between conductivity and durability.[20] Similar approaches have recently been applied to quaterphenyl isomers. Bakvand et al. investigated the effect of monomer configuration on poly(quaterphenyl piperidinium) AEMs using three isomeric quaterphenyl monomers (p,p-, p,m-, m,m-).[21] They reported that increasing the fraction of meta connectivity in the polymer backbone enhanced chain flexibility, which led to higher water uptake, improved hydroxide conductivity, and increased alkaline stability.

Although blending and copolymerization have been explored to modulate AEM properties, few studies have directly investigated the effect of backbone isomerism. For instance, Kim et al. and Mandal et al. examined other polymer classes, but did not focus on the conformational impact of isomeric backbone structures.[22,23]

Building on this, we systematically compare homopolymers, physical blends, and random copolymers of pyrrolidinium-functionalized membranes based on twisted m-terphenyl and linear p-terphenyl backbones to isolate the effects of molecular geometry and polymer integration on membrane morphology, mechanical strength, hydroxide conductivity, and AEMWE performance. Notably, this is the first direct comparison between physically blended and covalently copolymerized systems from distinct backbones. Our results reveal that combining m- and p-terphenyl units enables precise tuning between high ionic conductivity and mechanical robustness. This unified strategy establishes clear structure–property–performance correlations and offers a rational, scalable approach to designing next-generation AEMs with both efficient ionic transport and long-term stability in non-platinum group metal (non-PGM) electrochemical systems.

To achieve this, we employed a molecular design strategy using backbone isomerism to tune free volume and hydration in AEMs. Pyrrolidinium-functionalized membranes were synthesized via radical cyclopolymerization of diallylammonium monomers and chemically crosslinked with terphenyl backbones, forming a robust and stable network.[24] Ion exchange capacity was precisely controlled by incorporating diallyldimethylammonium chloride (DADMAC) during polymerization. By combining flexible m-terphenyl and rigid p-terphenyl units through homopolymerization, blending, and copolymerization, we systematically investigated the impact of isomeric geometry and polymer integration on membrane structure and performance.

2. Experimental

2.1. Materials

For the membrane preparation, dichloromethane (DCM, 99.5 %) was used by filtering after adding magnesium sulfate (MgSO4) supplied by Daejung and molecular sieve to remove moisture. Tetrahydrofuran (THF, 99.5 %), methyl alcohol (MeOH, 99.5 %), N-methyl-2-pyrrolidone (NMP, 99 %), dimethyl sulfoxide (DMSO, 99.5 %), ethyl ether (Ether, 99 %), 2,2'-azobis(2-methylpropionitrile) (AIBN, 99 %), and potassium hydroxide (KOH, 93 %) were supplied by Daejung and used. p-Terphenyl (PTP, ≥99.5 %), m-terphenyl (MTP, 99 %), diallylmethylamine (DAMA, 97 %), diallyldimethylammonium chloride (DADMAC, ≥ 97 %), butylated hydroxytoluene (BHT, 99 %), and DMSO-d6 (DMSO-d6, 99.9 atom% D) were supplied by Sigma Aldrich Chemical Co. Ltd and used as received. Trifluoromethanesulfonic acid (TFSA, >98 %) was obtained from Sejin CI (TCI). 7-Bromo-1,1,1-trifluoroheptan-2-one (96 %) was supplied by J&H Chem and chloroform-d6 ($CDCl_3$, atom% D) was supplied by Cambridge Isotope Laboratories, Inc. and used as received.

For membrane electrode assembly fabrication, iridium (IV) oxide (IrO_2, 99.99 wt%) and platinum ruthenium on carbon support (PtRu/C, Pt 50 wt%, Ru 25 wt%, C 25wt%) were purchased from Alfa Aesar. Isopropyl alcohol (IPA, 99 %) and ethyl acetate (EA, 99.5 %) were purchased from Daejung. Polyvinylbenzyl chloride (PVBC, 95 %), 2-(4-fluorophenyl)ethylamine (98 %), trimethylamine (TMA, 30-35 wt% solution in ethanol), Nickel(Ⅱ) chloride hexahydrate ($NiCl_2{\cdot}6H_2O$≥ 98 %), Iron(Ⅲ) chloride hexahydrate

($FeCl_3 \cdot 6H_2O$, ≥ 98 %, Sigma-Aldrich), Sodium borohydride ($NaBH_4$, ≥ 98 %) were purchased from Sigma Aldrich and used as received. FAA-3-50 and Pention-72–15CL membranes were purchased from Fumatech and Fuel Cell Store Co., Ltd., respectively, and used as reference membranes for benchmarking.

2.2. Synthesis of terphenyl-based polymers

The polymers were synthesized via a superacid-catalyzed polyhydroxyalkylation reaction, as previously reported,[25] using trifluoromethanesulfonic acid (TFSA) as a catalyst. In a 100 mL round-bottom flask (RB), PTP (4 g, 17.37 mmol) was dissolved in 16.8 mL of dichloromethane (DCM). To this solution, 7-bromo-1,1,1-trifluoroheptane-2-one (6.77 g, 27.38 mmol) was added, followed by the dropwise addition of TFSA (16.8 mL) under stirring in an ice bath. The reaction mixture was then allowed to gradually warm from 0 °C to room temperature over 4 h. During this period, the solution turned dark blue and developed a highly viscous texture, indicating the progression of polymerization. The resulting viscous polymer was precipitated in excess MeOH, redissolved in THF, and reprecipitated in MeOH. This purification cycle was repeated three times to remove unreacted monomers and byproducts. The final product, an ivory-colored polymer (denoted as PTP-$HBrF_3$), was collected by filtration and dried under vacuum at 80 °C for 12 h. The obtained polymer exhibited a yield of 89 %, indicating efficient polymerization under the employed conditions.

The quaternization of PTP-$HBrF_3$ was subsequently carried out to introduce anion exchange functionality via a Menshutkin reaction between the pendant alkyl halides and a tertiary amine.[26] Specifically, DAMA was reacted with PTP-$HBrF_3$ to yield the functionalized polymer, referred to as PTP-DAMA. In a 100 mL RB flask, PTP-$HBrF_3$ (1 g, 2.18 mmol) was dissolved in 20 mL of NMP. To this solution, BHT (0.230 g, 1.04 mmol) was added as a polymerization inhibitor to prevent undesired cross-linking of the DAMA. DAMA (0.97 g, 8.71 mmol) was then added slowly, and the reaction mixture was stirred at 50 °C for 5 d under a nitrogen atmosphere. After completion of the quaternization reaction, the polymer was precipitated in excess Ether, washed repeatedly with fresh Ether to remove residual amine, and dried under vacuum at room temperature for 3 h. The MTP-based polymer was synthesized following the same procedure as that of the PTP-based polymer. For the copolymer, a 1:1 molar ratio of MTP and PTP monomers was used under identical reaction conditions. This composition was selected to investigate the intermediate structural characteristics between the linear p-terphenyl backbone and the kinked m-terphenyl backbone and to evaluate the effect of backbone isomer incorporation on membrane properties. All polymers were obtained in yields of 64–90 %.

2.3. Synthesis of diallylammonium-based AEMs

PTP-DAMA-based AEMs with various theoretical ion exchange capacities (IECs), ranging from 1.97 to 3.24 meq g^{-1}, were prepared by cyclopolymerization. To fabricate the PTP-DAMA (3.24) membrane, synthesized PTP-DAMA (0.08 g, 0.15 mmol) was dissolved in DMSO (1.44 g), and DADMAC (0.03 g, 0.18 mmol) was dissolved in MeOH (0.12 g). The two solutions were combined and mixed thoroughly, followed by the addition of AIBN (0.009 g) as an initiator. The mixture was cast in a mold, dried under vacuum for 3–4 h to remove the solvent, and then polymerized at 80 °C for 24 h. Membranes with lower IECs (2.70, 2.36, and 1.97 meq g^{-1}) were prepared via the same procedure with adjusting the DADMAC content in molar ratios of 0.9:1, 0.6:1, and 0:1 (DADMAC: PTP-DAMA), respectively.

For MTP-DAMA, bMPTP-DAMA, and cMPTP-DAMA membranes, samples with various IECs were first prepared, but only those with the lowest and highest IECs—1.97 and 3.24 meq g^{-1}—were selected to compare the effect of polymer integration on membrane performance. These membranes were fabricated using the same cyclopolymerization method as for the PTP-DAMA membranes. For the membranes with an IEC of 1.97, only the synthesized polymer and AIBN were used without DADMAC. To obtain membranes with an IEC of 3.24, DADMAC was added in a 1.2:1 molar ratio (DADMAC: tertiary amine units) relative to the polymer.

To investigate the effect of polymer backbone structure on membrane properties, bMPTP-DAMA membranes were prepared as physical blends of MTP-DAMA and PTP-DAMA in a 1:1 molar ratio. This approach aimed to combine the structural features of each homopolymer, enabling the evaluation of synergistic effects on membrane performance.

Additionally, cMPTP-DAMA membranes, based on copolymers synthesized from MTP and PTP monomers at a 1:1 molar feed ratio, were fabricated to further assess the influence of covalently integrated mixed backbones. All procedures for membrane casting, solvent removal, and thermal polymerization were identical to those described for PTP-DAMA membranes.

2.4. Characterizations and measurements

To characterize the structure of polymers, 400MHz ^1H and ^{19}F nuclear magnetic resonance (NMR) (AVANCEIII700, Bruker Corporation) were employed in $CDCl_3$-d6 and DMSO-d6 at 25 °C. Fourier-transform infrared (FT-IR) spectra were obtained by using PerkinElmer FT-IR system (Spectrum-GX) with attenuated total reflectance (ATR) mode to analyze the structure of AEMs. The thermal stability of AEMs was examined by thermal gravimetric analysis (TGA, TA Instrument TGA 2950) at a heating rate of 10 °C min^{-1} under nitrogen (N_2) atmosphere, over temperature range from 30 to 700 °C. Differential scanning calorimetry (DSC) was carried out with a TA Instrument DSC Q20-1426 at a heating rate of 10 °C min^{-1} under an N_2 atmosphere. Mechanical properties of the membranes were measured using a universal tensile machine (Tinius Olsen H5K-T). Tensile strength tests were performed on sample (0.5 cm × 4 cm) at room temperature with a stretching speed of 10 mm min^{-1}. Dry-state measurements were conducted using membranes dried at 80 °C prior to testing. For wet-state measurements, the membranes were immersed in deionized water for 24 h to reach a fully hydrated state, removed from the water, and immediately subjected to tensile testing. Field Emission Scanning Electron

Microscopy (FE-SEM) images were obtained on an Inspect F50 (FEI, Korea) to verify the morphology of membranes on an Inspect F50 (FEI, Korea).

The theoretical IEC values were calculated based on the molecular weight of the repeating unit and the number of pyrrolidinium cationic groups incorporated per repeating unit. The IEC was determined by dividing the total number of cationic sites by the corresponding repeating-unit molecular weight.

The swelling ratio (SR) and water uptake (WU) were evaluated after immersing the membranes in water at room temperature for 24 h. After removal from the water, any excess water on the membrane surface was carefully wiped off, and the weight and length of the membranes were measured. The membranes were then dried completely, and their weight (W) and length (L) were again measured. The SR and WU were then calculated using the following equation:

$$SR = \left(L_{wet} - L_{dry}\right)/L_{dry} \times 100\ \%$$

$$WU = \left(W_{wet} - W_{dry}\right)/W_{dry} \times 100\ \%$$

KOH uptake was also tested in the same way as WU. the membranes were immersed in 1M KOH at room temperature for 24 h. After removal from the KOH solution, excess KOH was carefully wiped off, and the weight of membranes was measured. The membranes were washed several times with distilled water, dried completely, and their weight was measured. KOH uptake was then calculated using the following equation:

$$\text{KOH uptake} = \left(m_{wet,\,KOH} - m_{dry,\,KOH}\right)/m_{dry,\,KOH} \times 100\ \%$$

The hydration number (λ) defines the quantity of H2O molecules surrounding each cation. It was determined using WU and IEC. The λ was calculated by the following equation:

$$\lambda = 10 \times WU\ (\%) / (IEC \times 18)$$

One widely accepted method for calculating the fractional free volume (FFV) is that proposed by Lee.[27] In this approach, the density of the polymer is experimentally measured, and the occupied volume of the polymer chains is subtracted from the specific volume.[28] The specific free volume (SFV) and FFV can then be determined using the following equation:

$$SFV = V\text{-}V_0$$

$$FFV = (V\text{-}V_0) / V = 1\text{-}\rho V_0$$

Here, V represents the specific volume ($cm^3\ mol^{-1}$), and V_0 denotes the occupied volume of the polymer ($cm^3\ mol^{-1}$). The occupied volume is theoretically related to the van der Waals volume (V_{vdw}, $cm^3\ mol^{-1}$), which is estimated using the Bondi group contribution method. The relationship is expressed as follows:

$$V_0 = 1.3 \times V_{vdw}$$

The polymer density (ρ) ($g\ cm^{-3}$) can experimentally be measured and is calculated using the following equation:

$$\rho = W_{air} / \left(W_{air} - W_{liquid}\right) \times \rho_0$$

where W_{air} is the weight of the polymer measured in air, W_{liquid} is the weight measured in an auxiliary liquid, and ρ_0 is the density of the auxiliary liquid ($g\ cm^{-3}$).

Two types of water exist in AEMs: bound water and free water. Various techniques have been employed to investigate the structure and properties of water absorbed by hydrophilic polymers. Among these, thermal analysis offers several advantages, including qualitative evaluation of water content, minimal sample size requirements, and rapid measurement times.[29] In TGA thermograms, a two-step weight loss is typically observed, corresponding to the removal of free and bound water. The first weight loss occurs in the lower temperature range (below 100 °C) and is attributed to the evaporation of free water. The second weight loss takes place at higher temperatures (e.g., 100–200 °C) and corresponds to the removal of bound water, which is strongly associated with the polymer matrix.[30,31]

The in-plane hydroxide conductivity (σ) of the AEMs was measured in water at different temperatures by two-electrode electrochemical impedance spectroscopy (EIS, Solartron SI 1260). AEM samples (0.5 cm × 4 cm) were immersed in 1M KOH for at least 48 h to convert them into the OH^- form and were washed several times with distilled water. All samples were measured over a frequency range from 100 μHz to 13 MHz with an amplitude of 20 mV. Hydroxide conductivity was calculated using the following equation:

$$\sigma = L / (R \times d \times W)$$

Where L is the distance between two electrodes (cm), R is the measured ohmic resistance (Ω), d is the thickness of the membrane (cm), and W is the width of the membrane (cm).

2.5. Membrane-electrode assembly (MEA) fabrication and electrolysis performance

MEAs with a 1 or 5 cm^2 active area were fabricated using the catalyst-coated substrate (CCS) method. Platinum-ruthenium on carbon (PtRu/C) was used as the cathode catalyst, while iridium oxide (IrO_2) and nickel-iron (NiFe) were used as the anode catalysts. NiFe was synthesized in-house.[32] Catalyst inks were prepared by dispersing each catalyst powder in a TMA-70 ionomer solution that was synthesized in-house.[33] The TMA-70 ionomer solution was made by mixing a 5 wt% TMA-70 ionomer in a 1:1 volumetric ratio of IPA and water. The ionomer-to-carbon (I/C) weight ratio was set at 0.5, with a binder content of 10 wt% for the oxygen evolution reaction (OER) catalyst layer.

The catalyst inks were dispersed via ultrasonic treatment for more than 20 min, with the water temperature maintained below 30 °C to prevent catalyst agglomeration. The prepared catalyst inks were directly sprayed onto the gas diffusion layer (GDL) on a pre-heated hotplate at 70 °C to fabricate the gas diffusion electrodes (GDEs). The cathode catalyst loading was 0.6 mg Pt cm^{-2}, while the anode catalyst loading was 2.0 mg Ir cm^{-2} and 3.0 mg NiFe cm^{-2}. The fabricated CCS was dried at room temperature for over 1 h to remove residual solvent from the catalyst layers.

Before the single-cell application, terphenyl-based AEMs were sandwiched between the fabricated electrodes without undergoing a hot-pressing process. The AEM was placed between the GDEs and assembled into a single cell with Teflon gaskets, using 80 inch-pounds of torque. An electrolyte reservoir containing 500 mL of either pure water or a 1M KOH solution

was used, depending on the experimental conditions. For the pure water setup, the liquid was fed exclusively to the anode, while for the 1M KOH solution setup, the liquid was supplied to both the anode and cathode. The AEMWE performance was tested with a power supply provided by a Biologic SP-200 potentiostat, in conjunction with an HCV-3048 power booster.

3. Results and Discussion

3.1. Conceptual Design of Terphenyl-Based AEMs

In this study, we designed a series of AEMs using terphenyl-based backbones to investigate how backbone geometry influences membrane properties. Terphenyl exists in three positional isomers—ortho (o), meta (m), and para (p)—which differ in the relative orientation of their phenyl rings. Among them, MTP adopts a twisted, non-linear conformation, introducing irregularity and increasing the FFV of the polymer matrix. This feature is expected to promote water uptake and facilitate OH- transport by creating more accessible diffusion pathways. In contrast, PTP forms a linear, rod-like structure that allows for dense chain packing, potentially enhancing mechanical integrity but limiting hydration and ion transport. Excessive backbone distortion arises from the large steric hindrance caused by the tortuous o-terphenyl unit.[20] Consequently, the ortho isomer fails to form a homogeneous membrane and breaks into pieces after solution casting. Hence, o-terphenyl is not considered.

To systematically evaluate the effect of backbone geometry, AEMs were synthesized using either M- or P-TP monomers. In addition to homopolymer-based membranes, we prepared physical blends and statistical copolymers containing both isomers to examine how different modes of integration affect the resulting structure–property relationships. This approach enabled a direct comparison of how backbone conformation and polymer architecture affect hydration, conductivity, and mechanical performance.

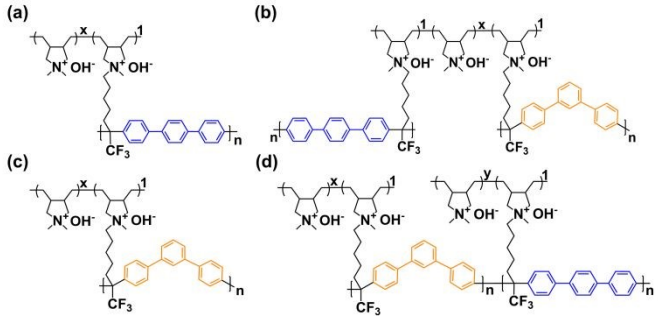

Figure 1. Design concept of terphenyl-based AEMs: (a) PTP-DAMA (b) bMPTP-DAMA (c) MTP-DAMA (d) cMPTP-DAMA

To introduce stable anion conducting functionalities, pyrrolidinium cation groups were incorporated through the cyclopolymerization of diallylammonium monomers. The resulting PDAA halides were crosslinked with the terphenyl-based polymer network to enhance structural integrity. The five-membered pyrrolidinium rings offer improved alkaline stability by resisting Hofmann elimination and nucleophilic attack. The IEC was systematically tuned by co-polymerizing DADMAC, with the theoretical IEC values ranging from 1.97 to 3.24 meq g^{-1}. These variations in IEC allowed investigation of their influence on water uptake and hydroxide conductivity, providing insights into hydration–transport relationships. In general, higher IECs resulted in greater water uptake and enhanced hydroxide conductivity, thereby supporting the analysis of how hydration levels affect ion transport.

By integrating rigid aromatic backbones with chemically stable QA groups in a modular framework, this system enables controlled investigation of how molecular geometry and polymer structure jointly govern AEM performance (Figure 1).

3.2. Synthesis and Structural Characterization of terphenyl-based AEM

To develop structurally robust and tunable AEMs, PTP and MTP monomers were selected as the polymer backbones due to their distinct geometric configurations. The synthesis of terphenyl-based AEM precursors began with a superacid-catalyzed hydroxyalkylation reaction between terphenyl and 7-bromo-1,1,1-trifluoroheptan-2-one, yielding trifluoromethylated intermediates: PTP-$HBrF_3$, MTP-$HBrF_3$, and cMPTP-$HBrF_3$ (Figure 2).

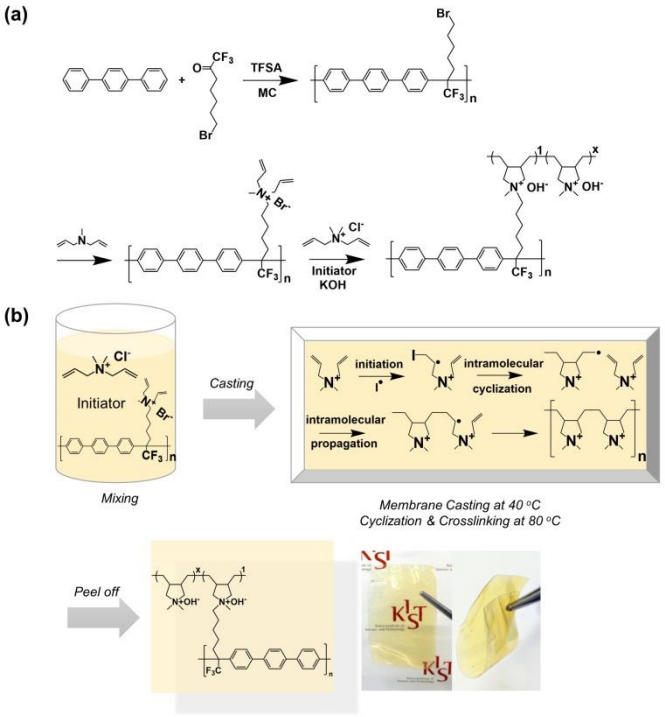

Figure 2. (a) Schematic diagram of the synthesis mechanism of the PDAA-based AEM and (b) membrane fabrication process

The chemical structures of the synthesized intermediates were confirmed by ^1H and ^{19}F NMR spectroscopy (Figure 3). The ^{19}F NMR spectra exhibited a sharp singlet near −65 ppm, indicating the presence of chemically equivalent CF_3 groups in the polymer chain (Figure S1). In the ^1H NMR spectra, the PTP derivative

showed three sets of doublets in the aromatic region (7.4–7.9 ppm), characteristic of the symmetric para-linked terphenyl structure, whereas the MTP derivative displayed multiplets, consistent with the twisted, less symmetric meta-terphenyl configuration. In addition, aliphatic protons adjacent to the ketone group appeared in the range of 1.3–3.4 ppm. Although PTP and MTP shared the same molecular formula, their different substitution patterns produced distinct NMR signals, allowing reliable identification of each component within the polymers. Distinct diagnostic peaks were clearly observed in both the homopolymer and copolymer spectra, and the integral ratios closely matched the monomer feed ratios. These results indicated that ^{1}H NMR analysis confirmed the successful synthesis of the polymers.

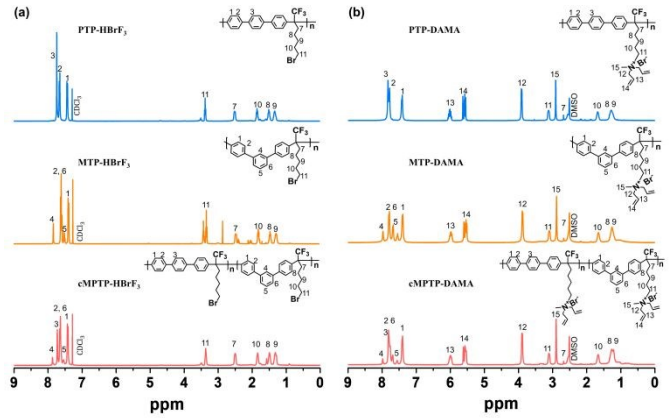

Figure 3. ^{1}H NMR spectra of (a) main backbones: PTP-HBrF_3, MTP-HBrF_3, cMPTP-HBrF_3 and of (b) ionic form polymers: PTP-DAMA, MTP-DAMA, cMPTP-DAMA

The weight-average molecular weights (Mw) of all terphenyl-HBrF_3 derivatives exceeded 100,000 g mol^{-1}, with polydispersity indices (PDI) of ~4–5 (Figure S2), suggesting sufficient chain entanglement for mechanical durability.[34,35] These precursors were then functionalized with DAMA via a Menshutkin reaction to form quaternizable intermediates—PTP-DAMA, MTP-DAMA, and cMPTP-DAMA. BHT was added during the reaction to inhibit premature radical polymerization of allyl groups. Successful incorporation of the DAMA groups was confirmed by the emergence of new 1H NMR signals between 5.5–6.1 ppm (vinylic protons), ~2.9 ppm (methyl protons), and ~4.0 ppm (methylene adjacent to nitrogen). A notable downfield shift was also observed in the methylene signals initially near 3.4 ppm (from –CH_2Br), which moved to ~3.0 ppm after substitution with the DAMA moiety, confirming the successful nucleophilic substitution (Figure 3b). The absence of unexpected signals in the ^{1}H NMR spectra indicated that no side reactions occurred. All synthesized terphenyl-DAMA derivatives exhibited good solubility in DMSO, demonstrating their suitability for further crosslinking, membrane casting, and physicochemical characterization.

The resulting membranes were labelled as PTP-DAMA (IEC), MTP-DAMA (IEC), bMPTP-DAMA (IEC), and cMPTP-DAMA (IEC), where the theoretical IEC is indicated in parentheses. Membranes were fabricated with IEC ranging from 1.97 to 3.24 meq g^{-1} depending on the ratio of DAMA to DADMAC (Table S1, S2). While increased DADMAC content theoretically allows higher IECs, excessive incorporation was found to compromise mechanical stability. A balance between ionic content and structural integrity was thus maintained, and the membrane with an IEC of 3.24 meq g^{-1} represented the upper limit of usable IEC under stable conditions. In comparison to commercial membranes such as Fumasep FAA-3 (IEC ~2.0 meq g^{-1}), Orion TM1 (IEC ~2.2 meq g^{-1}) or PiperION (IEC ~2.4 meq g^{-1}), the synthesized membranes offer significantly broader IEC tunability while maintaining high structural integrity.[36] Altogether, this synthetic strategy offers a robust and tunable framework for designing high-performance AEMs, with controlled backbone architecture and ion-exchange functionality tailored for fundamental and applied investigations.

To verify quaternization and track IEC-dependent functionalization, FT-IR spectroscopy was performed on representative samples: the unfunctionalized backbone, and two functionalized membranes with IECs of 1.97 and 3.24 meq g^{-1} membrane (Figure S3). In the spectrum of the unmodified backbone, a distinct aromatic C=C stretching vibration was observed at ~1500 cm^{-1}, confirming the presence of the terphenyl unit.[37] A sharp band at ~1140 cm^{-1} corresponds to C–F stretching in the trifluoromethyl-substituted backbone.[38] Upon DAMA functionalization via the Menshutkin reaction, absorption band at 1647 cm^{-1} appeared due to the C–N stretching of the QA group.[39] This peak increased in intensity with IEC, reflecting the extent of ion-exchange group incorporation.[40] Additionally, a weak absorption band at ~3080 cm^{-1}, corresponding to the =CH_2 stretching vibration of the terminal allyl group, was observed in the unreacted PTP-DAMA precursor. This intensity disappeared completely, indicating the successful cyclopolymerization of the diallyl groups, resulting in a stable crosslinked membrane network.

SEM analysis revealed that all membrane samples exhibited smooth, homogeneous surfaces without visible defects, domain formation, or phase separation (Figure S4, S5). This uniformity suggests that the polymers were well-dispersed and cast consistently during membrane fabrication, ensuring reproducibility and film integrity. Cross-sectional SEM images of AEMs confirmed dense, void-free internal structures, indicative of strong polymer cohesion and effective film formation. This morphological uniformity ensures dimensional stability and minimizes undesired swelling during hydration. Such compact, defect-free architectures are critical for consistent ion transport and long-term mechanical reliability under operating conditions relevant to fuel cells or water electrolyzers.

3.3. Thermal and Mechanical Properties of AEMs

AEMWE typically operate under harsh electrochemical conditions, often at elevated temperatures ranging from 60 to 80 °C. Therefore, thermal and mechanical stability are critical for ensuring long-term membrane durability.

TGA was conducted to assess the thermal decomposition behavior of the synthesized terphenyl-based AEMs (Figure 4a,

View Article Online DOI: 10.1039/D6TA02921D

b). An initial weight loss observed below 250 °C is attributed to the degradation of thermally sensitive QA groups. Further decomposition at higher temperatures corresponds to backbone degradation. All membranes remained thermally stable above 150 °C, confirming their applicability for AEMWE operation up to 100 °C.

DSC was used to determine the glass transition temperature (Tg) of the membranes (Figure 4c, d). All membranes showed Tg values in the range of 80–92 °C. A referenced study reported that membranes with similar Tg (~80 °C) remained mechanically and chemically stable during 1000 h of operation at up to 95 °C, with minimal changes in IEC, molecular weight, and weight loss.[41] These findings suggest that the membranes developed here, with Tg values above 80 °C and reinforced by crosslinking and poly(DADMAC), are likely to maintain stable AEMWE performance above 80 °C. Tg increased with higher poly(DADMAC) content and crosslink density, due to reduced chain mobility and enhanced rigidity. This is consistent with prior studies; for example, Yagizatli et al. reported that thermal crosslinking in SPEEK-PVA blend membranes increased Tg due to constrained segmental motion within the crosslinked domains.[42] The higher Tg observed in MTP homopolymers compared to their PTP analogs can be attributed to the increased conformational restriction and reduced chain mobility resulting from the non-linear, kinked backbone structure of the meta-linkage.[43] In contrast, polymer blends often exhibit a lower Tg than their respective homopolymers due to weakened intermolecular interactions and increased free volume with changing packing density, which facilitate segmental motion and reduce the energy barrier for glass transition.[44] Among low-IEC membranes, The exceptional Tg of cMPTP-DAMA originates from the synergistic effects of linear rigidity PTP and 3D conformational restriction MTP, which together suppress segmental motion. This mechanism parallels the Tg enhancement observed in sulfone-containing oxyethylene copolymers, where reduced free volume—whether structurally or chemically induced—leads to increased thermal resistance.[45] Notably, cMPTP-DAMA achieves such thermal stability without relying on strong polar interactions, offering a novel design paradigm for thermally robust polymers in low-IEC applications. For high-IEC membranes, Tg further increased—reaching 92 °C in cMPTP-DAMA—driven by both higher crosslink density and potential ionic clustering effects. This behavior is consistent with previous findings by Spring et al., who reported that copolymerization of rigid norbornene-dicarboximide monomers resulted in Tg enhancement due to restricted segmental motion and reduces conformational entropy.[19,46] The Tg values observed in this study (~80–92 °C) are comparable to those reported for polyketone-based AEMs designed for alkaline electrolysis by Racchi et al., where similar crosslinking effects and backbone rigidity contributed to thermal resistance.[47]

Mechanical strength was evaluated via tensile testing under fully hydrated conditions (Figure 4e, f). As expected, membranes with higher IEC (3.24 meq g^{-1}) showed reduced tensile strength due to increased water uptake and plasticization by ionic groups.[48] The flexible nature of poly(DADMAC) further contributed to reduced modulus.[9] Among all samples, PTP-DAMA membranes exhibited the highest tensile strength (up to 45 MPa at IEC = 1.97), benefiting from the linear, rigid PTP backbone and relatively low water uptake, which helps maintain dense chain packing. In contrast, MTP-DAMA membranes were the weakest, reflecting the more flexible backbone, higher water uptake, and lower chain packing density. The observed strength of 45 MPa under wet conditions compares favorably to that of commercial or literature membranes. For instance, Khalid et al. reported a tensile strength below 20MPa for a wer-state PiperION PI-20 (IEC ~2.3 meq g^{-1}).[48] Also, Orion TM1 (IEC ~2.2 meq g^{-1}) exhibit wet-state strengths below 30 MPa, PTP-DAMA show enhanced resilience under operationally relevant, hydrated conditions.[36] Blended (bMPTP-DAMA) and copolymerized (cMPTP-DAMA) membranes showed intermediate mechanical strengths between those of PTP- and MTP-DAMA membranes.[49] Notably, cMPTP-DAMA generally exhibited higher tensile strength than bMPTP-DAMA, suggesting that covalent incorporation of m- and p-terphenyl units can improve structural robustness compared to physical blending. However, this improvement was accompanied by a trade-off between strength and ductility, particularly at higher IEC values.

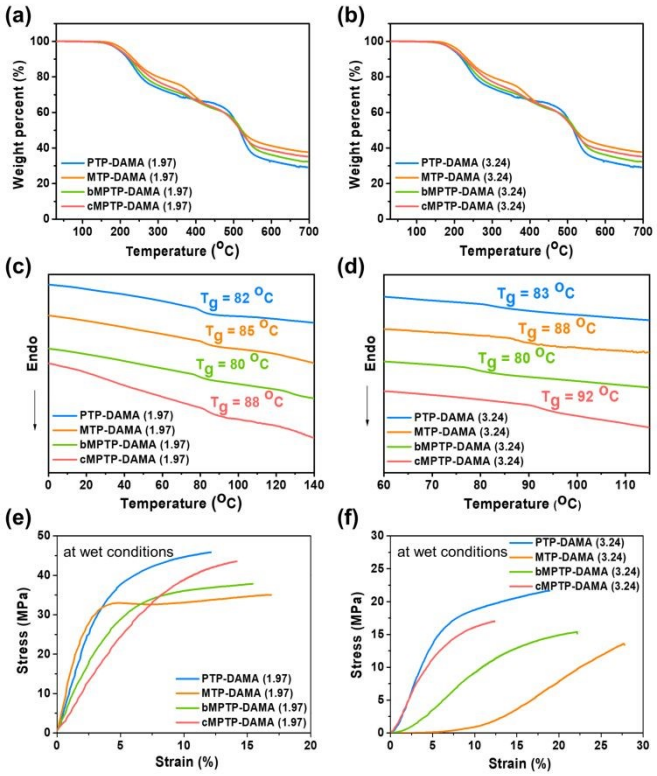

Figure 4. Thermal and mechanical properties of IEC 1.97 membranes: (a) TGA curves of IEC 1.97 membrane (b) TGA curves of IEC 3.24 membrane (c) DSC curves of IEC 1.97 membranes (d) DSC curves of IEC 3.24 membranes (e) strain-stress curves of IEC 3.24 membrane (f) strain-stress curves of IEC 3.24 membrane

The mechanical strength trends observed under hydrated conditions were preserved even in the dry state (Table S3). This

View Article Online
DOI: 10.1039/D5TA03024H

trend is consistent with prior findings by Kim et al., who found that main-chain conjugated copolymers exhibited superior mechanical properties compared to polymer blends, owing to improved phase continuity and stronger interchain interactions.[50] During cell assembly, significant compressive forces are applied, and membranes with insufficient modulus may undergo deformation, potentially leading to performance degradation or mechanical failure. Therefore, in addition to electrochemical performance, the mechanical properties of the membranes—particularly the modulus—are critical for practical application. As shown in Table S3, PTP-DAMA (1.97) exhibited the highest modulus of 5.82 MPa, indicating superior resistance to compression. In contrast, MTP-DAMA (3.24) showed a notably low modulus of 0.85 MPa, suggesting a higher likelihood of deformation under stress. These results highlight the importance of considering mechanical robustness alongside ionic conductivity when designing membrane materials.

The differing trends between Tg and mechanical properties can be interpreted as arising from the fact that these properties are influenced by distinct structural and environmental factors. Tg primarily reflects the rigidity and internal mobility of the polymer chains, which explains why the copolymer exhibits the highest Tg. In contrast, mechanical properties are governed not only by water uptake but also by the polymer's microstructure, isomerism, phase separation, and crystallinity. Notably, even under dry conditions where the effect of water is eliminated, mechanical properties still differ from Tg trends because PTP possesses a more regular and robust chain arrangement with higher crystallinity, resulting in superior mechanical strength. Therefore, while Tg reflects the chain mobility of the polymer, mechanical properties can be interpreted as determined by the complex interplay of the polymer's overall microstructure and intermolecular interactions, leading to the observed discrepancy between the two sets of results.

3.4. Hydration properties of AEMs

Hydration behavior is a key determinant of ion conductivity, dimensional stability, and mechanical performance in AEMs. The ability of a membrane to absorb and manage water directly influences ion mobility and structural robustness under hydrated operating conditions, such as those encountered in AEMWE. In this study, the hydration properties of terphenyl-based AEMs were evaluated in relation to their IEC, backbone geometry, and polymer architecture (homopolymer, blend, or copolymer).

Figure S6 shows that both water uptake and swelling ratio of PTP-DAMA membranes increased proportionally with IEC, ranging from 1.97 to 3.24 meq g^{-1}. This trend is expected, as a higher concentration of QA groups enhances hydrophilicity and attracts more water into the polymer matrix.[51] A similar pattern was observed in KOH uptake (Table S5), indicating that increased IEC not only raises water affinity but also improves OH^- accommodation.

To assess the effect of polymer backbone structure on hydration behavior, we compared the water uptake and swelling ratio of AEMs (Figure 5a, b). All terphenyl-based membranes exhibited lower water uptake values compared to poly(m-terphenyl-co-p-terphenyl)-based AEMs with piperidinium/spirocyclic cations previously reported by Zhang et al (35~41 %).[52] This was attributed to the distinct rigidity and compactness of the pyrrolidinium-based cation formed via cyclopolymerization. The resulting rigid and densely packed ionic network reduced water uptake despite comparable backbone composition. Moreover, the terphenyl-based membranes also demonstrated significantly lower swelling ratios compared to Zhang et al.'s membranes, highlighting their superior dimensional stability.[36] In AEM applications, excessive swelling can compromise membrane integrity and mechanical strength; thus, this reduced swelling behavior is particularly advantageous for long-term electrochemical operation.

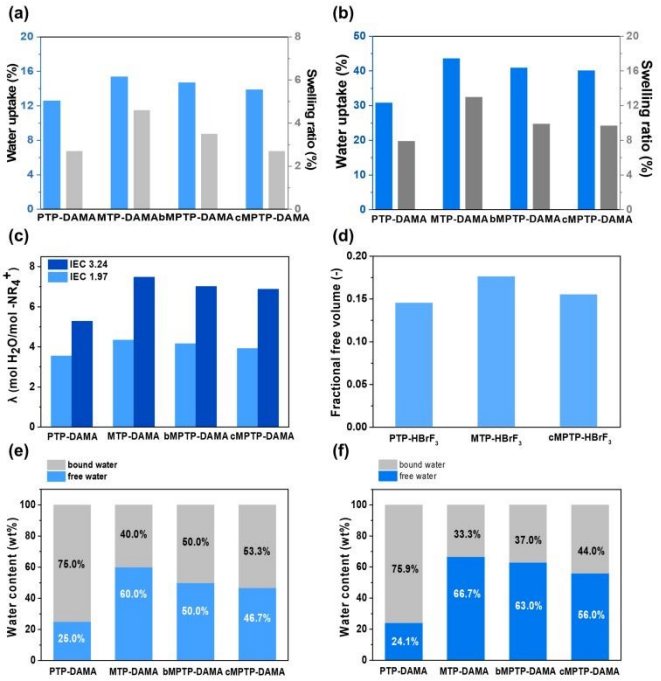

Figure 5. Hydration properties: (a) water uptake and swelling ratio of IEC 1.97 membranes (b) water uptake and swelling ratio of IEC 3.24 membranes (c) hydration number of IEC 1.97 and 3.24 membranes (d) fractional free volume (FFV) of the polymer (e) free water content of IEC 1.97 membranes (f) free water content of IEC 3.24 membranes

As shown in Figure 5a and 5b, MTP-DAMA exhibited the highest water uptake and swelling ratio among all membranes. At IEC 3.24 meq g^{-1}, water uptake reached 43.6 % and swelling ratio reached 13.0 %. This is attributed to the flexible and twisted structure of mTP, which reduces chain packing density and increases FFV, facilitating water absorption and the formation of ionic clusters.[19,20] In contrast, PTP-DAMA showed significantly lower water uptake (30.8 %) and swelling ratio (7.9 %) at the same IEC. The rigid, linear pTP units promote tight chain packing and limit the formation of microvoids, restricting water ingress and minimizing dimensional changes upon hydration. These architectures incorporate both rigid and flexible components and enable a tunable balance between water absorption and dimensional stability. Due to the incorporation of both MTP and PTP units, bMPTP-DAMAs and cMPTP-

View Article Online DOI: 10.1039/D5TA03934H

DAMAs exhibit intermediate water uptake and swelling ratios compared to those of MTP-DAMAs and PTP-DAMAs. Notably, cMPTP-DAMA exhibited slightly lower swelling than bMPTP-DAMA, despite similar water uptake levels (Table S5). This difference is attributed to the covalent integration of PTP and MTP in the copolymer backbone, which suppresses macroscopic phase separation and promotes more uniform microphase distribution.[47,53]

As shown in Figure 5c, the superior water uptake of the MTP-DAMA membranes was further confirmed by measurements of their hydration number (λ), which denotes the number of water molecules associated with each ion-exchange site. At IEC 3.24, MTP-DAMA showed a λ of 7.48, compared to 5.28 for PTP-DAMA. At lower IEC (1.97), the λ values were 4.34 and 3.55, respectively. These results indicate that mTP-based membranes form larger hydration shells, likely due to their greater FFV and disordered chain conformation. The enhanced rotational freedom in mTP units facilitates the accommodation of water molecules around the cationic sites, forming well-hydrated, dynamic ionic domains.[19] In contrast, the PTP-DAMA membranes, composed of the rigid and linear PTP backbone, displayed the lowest λ values across both IEC levels. The extended, linear structure of pTP promotes dense chain packing and reduces the accessibility of water molecules to the ionic sites, thereby limiting hydration. Hybrid membranes—bMPTP-DAMA and cMPTP-DAMA—which incorporate both mTP and pTP units, exhibited intermediate hydration numbers. Their λ values were lower than those of the MTP-DAMA membranes but higher than those of the PTP-DAMA membranes. It is considered that the similar hydration properties observed in both bMPTP-DAMA and cMPTP-DAMA are due to the identical ratio of MTP and PTP incorporated into both systems, resulting in a similar distribution of hydrophilic and hydrophobic regions. Although other factors may also contribute, this distribution is likely the main factor behind the negligible differences in their physical properties.

Fractional free volume (FFV) is a key parameter for understanding the transport properties of polymer membranes. Among various approaches for its estimation, molecular dynamics (MD) simulations allow for the direct evaluation of FFV at the atomic level by explicitly modeling the polymer structure. In these simulations, polymers are represented in either a fully atomistic or coarse-grained framework, and the system is equilibrated under appropriate temperature and pressure conditions. The accessible free volume can be calculated using probe-based techniques, in which a virtual probe of a defined size is inserted into the polymer matrix to identify void spaces that are sufficiently large to accommodate diffusing molecules. Alternatively, FFV can be estimated by subtracting the polymer's van der Waals volume from the total system volume, thereby defining the fraction of unoccupied volume.[54] Through these analyses, MD not only yields quantitative estimates of FFV but also allows the examination of how specific molecular features, such as backbone stiffness, tacticity, and bulky side groups, influence the free volume landscape within polymer membranes.

In this study, the FFV of the polymers was calculated using Lee's free volume method.[27] The van der Waals volume of the polymer was determined based on the atomic group contributions reported by Wu et al..[55] The occupied volume was subsequently obtained using the Bondi group contribution approach. Polymer density was determined experimentally by measuring the weight of the samples in air and in an auxiliary liquid (water), from which the specific volume was calculated.[28] The FFV was then derived as the difference between the specific volume and the occupied volume, normalized by the specific volume. Figure 5d illustrates the calculated FFV of the backbone polymers PTP-$HBrF_3$, MTP-$HBrF_3$, and cMPTP-$HBrF_3$, with FFV values of 12 %, 15 %, and 14 %, respectively. Higher FFV allows for greater water retention and facilitates the formation of interconnected ionic channels. These channels are essential for sustaining high ion conductivity under hydrated conditions, especially in systems operating via the Grotthuss and vehicular transport mechanisms.[18,56] These differences in FFV are closely correlated with the hydration and ion transport properties of the corresponding membranes. The greater free volume in MTP-based membranes enables enhanced water retention and promotes OH^- mobility, thereby contributing to their superior ionic conductivity. Meta-linked backbones generally introduce a more kinked structure, leading to higher free volume and better-connected ion channels, which in turn promote water uptake and hydration. This trend is consistent with previous findings in poly(binaphthyl-co-terphenyl)-based AEMs, where m-terphenyl and p-terphenyl units were selectively incorporated into the copolymer backbones to yield QBNmTP and QBNpTP, respectively. The QBNmTP (m-linked) membrane exhibited greater free volume, more defined ion-channel morphology in XRD, and higher water uptake compared to its para-linked counterpart, QBNpTP.[20] Also, this structure–property relationship aligns well with prior findings, such as those by Yuan et al., who reported that the incorporation of hyperbranched architectures into AEMs significantly increased FFV and led to substantial improvements in hydroxide conductivity.[57]

Water within AEMs can be classified into "free" and "bound" components, each influencing conductivity and mechanical integrity differently. Free water does not interact with ionic conductors, while bound water is tightly bound to the membrane through interactions with the conductors.[29] Hydroxide ions primarily migrate through free water, which facilitates more efficient ion transport compared to bound water.[58] Free water facilitates rapid ion mobility and contributes to membrane flexibility, while bound water is tightly associated with ionic sites and can restrict ion transport and induce brittleness if dominant. Therefore, maintaining an optimal balance between free and bound water is essential to achieve high conductivity without sacrificing structural integrity.[59]

Various analytical techniques have been developed to elucidate the states of water within hydrated polymer membranes beyond gravimetric measurements. Low field nuclear magnetic resonance (LF NMR) relaxation measurements, performed in the time-domain (TD) mode, can differentiate water populations based on their molecular mobility. The transverse relaxation time (T_2) was measured using low-field NMR (LF-NMR) relaxometry.[60] The magnetization decay curves were acquired

using the Carr-Purcell-Meiboom-Gill (CPMG) pulse sequence. The resulting data were processed via Inverse Laplace Transform (ILT) to obtain the T_2 relaxation time distributions, which characterize the different states of water within the samples. Water molecules that are strongly associated with the polymer matrix exhibit restricted motion and correspondingly shorter transverse relaxation times (T_2). In contrast, more mobile, bulk like water shows longer T_2 values.[61] This approach provides insight into water–polymer interactions and mobility regimes within the membrane network that are not readily accessible from simple mass loss measurements. DSC offers a complementary thermal perspective on water state analysis by probing phase transitions of the absorbed water. In hydrated membranes, free water exhibits a melting endotherm near 0 ℃, which is comparable to that of bulk water. Bound water, on the other hand, interacts with polymer functional groups or is confined in nanoscale domains, resulting in depressed or broadened melting transitions at lower temperatures. Non-freezing bound water may not exhibit a detectable phase change under typical DSC conditions. By integrating the enthalpy associated with these thermal events, the relative amounts of free and bound water can be estimated in a semi quantitative manner.[29] This approach complements spectroscopic or relaxation-based measurements and aids in the interpretation of water–polymer interactions.

In our study, TGA was used to assess the free and bound water content of the membranes. TGA analysis of water content in the samples only provides a qualitative comparison, without the inclusion of quantitative measurements.[29] TGA-derived analysis (Figure 5e, f; Figure S7) showed that MTP-DAMA membranes possessed the highest free water content, followed by bMPTP-DAMA, cMPTP-DAMA, and finally PTP-DAMA. The enhanced free water content in MTP-DAMA is attributed to its open, kinked backbone that promotes hydration shell development and microvoid formation. Notably, bMPTP-DAMA consistently exhibits slightly higher values than cMPTP-DAMA, which can be attributed to more pronounced phase separation in the physically blended system.[22] This enhanced microphase separation in bMPTP-DAMA can facilitate the formation of well-defined ionic domains and water channels, thereby improving hydration and ion conductivity.[57] However, this increased phase separation may compromise mechanical strength, leading to a trade-off between ionic conductivity and mechanical stability. Li et al. systematically investigated the effect of free water on the mechanical properties of poly(vinyl alcohol), demonstrating that even a small amount (1.8 wt%) of water can reduce tensile strength by ~32 %, while significantly enhancing ductility by more than 2.5 times. This was attributed to the plasticizing and lubricating effect of free water, which disrupts inter-chain hydrogen bonding and increases chain mobility.[62]

3.5. Hydroxide Conductivity and Alkaline stability of AEMs

Hydroxide conductivity is one of the most critical performance metrics for AEMs, as it directly governs electrochemical efficiency in AEMWEs. Hydroxide conductivity of the PTP-DAMA membranes, measured in pure water across the temperature range of 25–80 °C, is shown in Figure S6. Conductivity increased with IEC due to the greater number of QA groups, which support more efficient OH^- transport by forming denser and more connected ionic channels.[50]

Figure 6a and b presents the hydroxide conductivity of all AEMs with various polymer backbones. As expected, all membranes exhibited Arrhenius-type thermally activated behavior, with conductivity increasing with temperature due to enhanced ion mobility and diffusion rates in the hydrated matrix. Among the series, MTP-DAMA membranes consistently demonstrated the highest conductivity across all temperatures and IEC values. At 80 °C and IEC 3.24 meq g^{-1}, MTP-DAMA achieved a conductivity of 112.56 mS cm^{-1}, outperforming bMPTP-DAMA (78.44 mS cm^{-1}), cMPTP-DAMA (53.64 mS cm^{-1}), and PTP-DAMA (48.51 mS cm^{-1}). Even at IEC 1.97 meq g^{-1}, MTP-DAMA exhibited 61.10 mS cm^{-1}, more than double that of PTP-DAMA (25.12 mS cm^{-1}). This trend mirrors the hydration behavior discussed earlier, underscoring the role of backbone geometry in governing water uptake and ion transport. This exceptional performance can be attributed to the contorted and flexible structure of the MTP backbone, which enhances free volume and hydration, thereby promoting the formation of well-connected ionic domains. This observation aligns with findings by Wu et al., who reported that a branched poly(terphenyl piperidinium) AEMs (b-PTP-2.5) membrane maintained high conductivity (~145 mS cm^{-1} at 80 °C) even with a 28 % reduction in water uptake, owing to enhanced free volume and ion transport channels formed through chain entanglement and branched architecture.[63]

For context, the commercial AEMs such as Orion and PiperION typically exhibit hydroxide conductivities of 112 mS cm^{-1} and 150 mS cm^{-1} at 80°C, respectively, with water uptake values of approximately 44 % and 50 %.[30,64] Remarkably, MTP-DAMA (3.24) shows a comparable conductivity to to the commercial AEM Orion, achieving 112.56 mS cm^{-1} at 80°C, with a comparable water uptake of approximately 43.6 %. Although the conductivity of MTP-DAMA (3.24) was slightly lower than that of PiperION, its superior mechanical properties suggested that future improvements in conductivity can be achieved with higher IEC values in future iterations. While the high IEC of MTP-DAMA (3.24) undoubtedly contributes to its high hydroxide conductivity, the membrane's superior performance cannot be solely attributed to IEC. This enhanced performance can be attributed to the molecular design of MTP-DAMA, which incorporates a twisted m-terphenyl backbone that increases the intrinsic free volume and facilitates the formation of well-connected ionic domains. These structural features enhance the mobility of hydroxide ions by promoting the formation of continuous ion transport pathways and increasing the proportion of free water molecules that contribute more effectively to ion conduction. Even at a lower IEC, MTP-DAMA (1.97) maintained high conductivity (61.10 mS cm^{-1}) with significantly reduced water uptake (~15.4 %), indicating efficient ion transport under moderate hydration. The bMPTP-

View Article Online DOI: 10.1039/D6TA02348B

DAMA membranes consistently outperformed cMPTP-DAMA membranes, which is likely due to the more pronounced microphase separation in the physically blended system. This structural feature is known to promote the formation of well-connected ionic domains, thereby improving OH^- conduction.

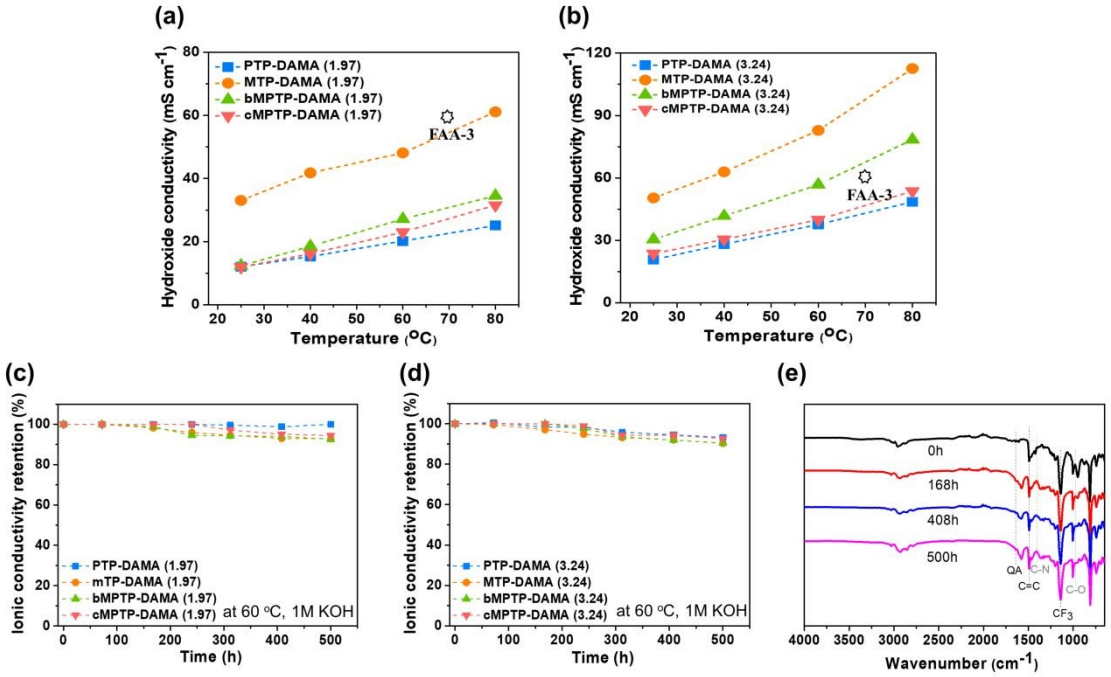

Figure 6. Ionic conductivity and alkaline stability of membranes (a) ionic conductivity of IEC 1.97 membranes (b) ionic conductivity of IEC 3.24 membranes (c) ionic conductivity retention of IEC 1.97 membranes (d) IEC 3.24 membranes (e) FT-IR spectra before and after alkaline stability test

The chemical durability of AEMs is a key determinant of the long-term operational stability of AEMFCs and related electrochemical systems. Under alkaline conditions, OH^- can degrade both the cationic groups and polymer backbone, especially at elevated temperatures.[65] This leads to a gradual decline in IEC and conductivity, along with reduced water retention and compromised mechanical stability.[66] Over time, such degradation may also increase cell voltage and lower hydrogen production efficiency.[67]

The chemical durability of the membranes was evaluated by immersing them in 1 M KOH at 60 °C for 500 h and periodically measuring hydroxide conductivity (Figure 6c, d). All membranes exhibited excellent conductivity retention, with values remaining above 90 %. In the IEC 1.97 group, PTP-DAMA showed the highest retention (98.0 %), followed by cMPTP-DAMA (94.5 %), bMPTP-DAMA (92.6 %), and MTP-DAMA (90.3 %). This stability is particularly advantageous under the high pH and temperature conditions encountered in alkaline electrolyzers and AEMFCs. In the higher IEC 3.24 group, a similar trend was observed. PTP-DAMA again demonstrated the greatest stability (93.3 %), whereas MTP-DAMA exhibited slightly lower retention (90.3 %). The slightly lower retention of MTP-DAMA is attributed to its more hydrated and open microstructure, which increases hydroxide accessibility and may accelerate degradation. In contrast, the rigid and tightly packed structure of PTP-DAMA restricts hydroxide diffusion and thus suppresses nucleophilic attack, offering better long-term alkaline stability. Khalid et al. measured hydroxide conductivity reduction in water by immersing commercial AEMs in 1 M KOH at 60 °C for 4 weeks.[48] Their results showed that the unreinforced PiperION membrane (20 μm) experienced a 60 % loss. Orion membrane, made from m-terphenyl with alkyl quaternary ammonium groups, demonstrated 40 % conductivity degradation after 4 weeks in an alkaline environment. While our results exhibited lower alkaline stability compared to piperidinium-based AEMs in other studies and commercial AEMs, the introduction of crosslinking and other stabilizing strategies has mitigated the degradation of pyrrolidinium-based AEMs.[17,68] Although the stability of pyrrolidinium-based AEMs remains a limitation, this study demonstrated the potential for improving alkaline stability through structural optimization.

These observations reflect a well-established trade-off between conductivity and chemical robustness in AEM design. Highly hydrated and flexible architectures promote ionic mobility but also expose vulnerable sites to degradation. Conversely, denser, rigid structures mitigate such reactions by limiting OH^- accessibility and local pH gradients. The bMPTP-DAMA and cMPTP-DAMA provided intermediate properties between MTP and PTP. The bMPTP-DAMA, exhibited moderate improvements in conductivity and hydration while maintaining good chemical stability, suggesting a favorable balance between free volume and mechanical integrity. Meanwhile, cMPTP-DAMA, offered enhanced alkaline durability but at the cost of slightly reduced hydroxide conductivity, due to restricted chain mobility and limited water uptake.

View Article Online
DOI: 10.1039/D6TA02934H

The chemical integrity of the membranes was further validated by FT-IR spectroscopy (Figure 6e). No new peaks or disappearance of existing bands was observed after 500 h in 1 M KOH, indicating that both the polymer backbones and pyrrolidinium-based QA cations remained intact. This observation confirms the structural integrity of the membranes under prolonged alkaline conditions and supports their excellent chemical stability. These findings were consistent with previous studies by Gjoshi et al., which demonstrated the excellent chemical stability of pyrrolidinium-based AEMs under alkaline conditions. Their study reported with only a 13 % reduction in conductivity observed after one month immersed in 2M KOH.[17]

3.6. AEMWEs Performance and Durability of terphenyl-based Membranes

AEMs operate under demanding electrochemical conditions, including elevated temperatures (60–90 °C), highly alkaline environments, applied potentials, and continuous hydration. While in-situ conductivity measurements offer a closer approximation to actual cell behavior than ex-situ methods, they still fall short of capturing the complex interplay of membrane–electrode interactions, gas crossover, and water management under real AEMWE operating conditions. Therefore, MEA testing is essential to evaluate practical applicability, providing comprehensive insights into system-level resistance, charge transfer, and long-term durability.

In this study, AEMWE performance was assessed through linear sweep voltammetry (LSV) in both 1 M KOH and pure water at 80 °C. PtRu/C and IrO_2 were employed as cathode and anode catalysts, respectively, in the PGM anode, while NiFe was used as a non-PGM anode catalyst. All membranes were fabricated with a thickness of 30–40 μm to minimize ohmic resistance and facilitate water transport.[63,69] EIS at 1.8 V revealed distinct semicircles in the Nyquist plots corresponding to ohmic (high-frequency intercept), charge-transfer (mid-frequency arc), and mass-transport resistance (low-frequency tail).[70,71]

Under PGM-catalyzed conditions, the MTP-DAMA (IEC 3.24) exhibited the highest cell performance, achieving a peak current density of 4.4 A cm^{-2} at 2.0 V (Figure 8a). This was significantly higher than that of the PTP-DAMA counterpart (1.5 A cm^{-2}). Blended and copolymer membranes, bMPTP-DAMA and cMPTP-DAMA, delivered intermediate performances of 3.1 and 2.2 A cm^{-2}, respectively. These results were mirrored in the low IEC group (1.97 meq g^{-1}), where MTP-DAMA still achieved the highest current density (4.04 A cm^{-2}), followed by bMPTP-DAMA, cMPTP-DAMA, and PTP-DAMA (1.1 A cm^{-2}) (Figure 8b). All terphenyl-based AEMs exhibited superior performance compared to the commercial PiperION membrane. According to Tricker et al., the PiperION membrane (40 μm) achieved a peak current density of approximately 2.5-2.9 A cm^{-2} at 2.0 V, 80 ℃ under PGM-catalyzed condition, which is lower than the current density of MTP-DAMA (3.24) (4.04 A cm^{-2}).[72]

The increase in IEC by DADMAC addition was accompanied by enhanced crosslinking through cyclopolymerization. This increased crosslinking density restricted the segmental mobility of polymer chains and suppressed water uptake and constrained ion transport. As a result, even with a substantially higher IEC, the AEMWE performance exhibited negligible variation between membranes with IECs of 1.97 and 3.24 mmol g^{-1}.

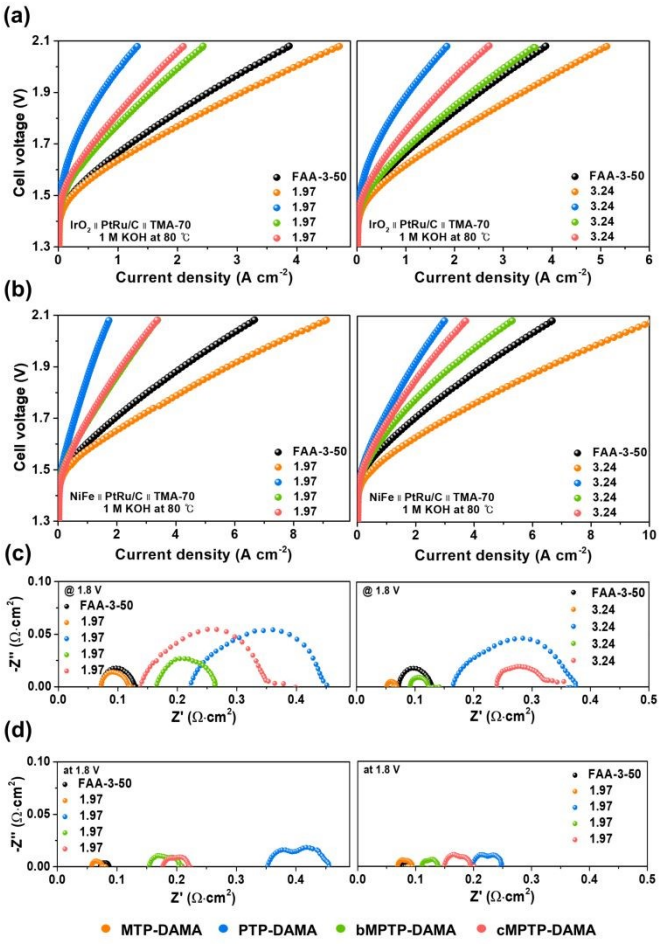

Figure 7. Comparison of performance in 1 M KOH-fed. (a) LSV curves of IEC 1.97 (left) and IEC 3.24 (right) membranes with PGM electrode (b) LSV curves of IEC 1.97 (left) and IEC 3.24 (right) membranes with non-PGM electrode (c) Nyquist plot of the of IEC 1.97 (left) and IEC 3.24 (right) membranes showing ohmic resistance with PGM electrode (d) Nyquist plot of of IEC 1.97 (left) and IEC 3.24 (right) membranes with non-PGM electrode

EIS measurements confirmed that MTP-DAMA membranes exhibited the lowest ohmic resistance (0.05–0.07 Ω cm^2), which can be attributed to their enhanced hydroxide conductivity, higher fractional free volume, and superior hydration (Figure 8c). The outstanding cell performance of MTP-DAMA is rooted in its molecular architecture. The contorted MTP backbone promotes the formation of well-connected ionic clusters with reduced tortuosity, enabling efficient long-range OH^- transport. Moreover, the flexible chain conformation helps sustain hydration shells near cationic sites, preserving ion conductivity even under lower water content. These structural features explain the low membrane resistance and high current output in both low and high IEC conditions.

View Article Online
DOI: 10.1039/D6TA02924H

Under non-PGM anode conditions, MTP-DAMA (3.24) again demonstrated exceptional performance, reaching 8.6 A cm^{-2} at 2.0 V—significantly surpassing the commercial FAA-3-50 membrane (~5.0 A cm^{-2}) and PTP-DAMA (2.5 A cm^{-2}) under identical conditions (Figure 8b). bMPTP-DAMA (3.24) and cMPTP-DAMA (3.24) showed intermediate values (4.3–3.1 A cm^{-2}). Notably, even at IEC 1.97, MTP-DAMA achieved 7.7 A cm^{-2}, maintaining low ohmic resistance (0.06 Ω cm^2) (figure 8d). These results affirm the scalability and competitiveness of MTP-DAMA in AEMWE systems employing a non-PGM anode.

The intermediate performances of bMPTP-DAMA and cMPTP-DAMA also highlight the benefits of blending and copolymerization strategies in tuning AEM properties. In the case of bMPTP-DAMA, partial incorporation of the MTP segment through blending allowed improved phase compatibility while retaining a portion of the favorable ionic connectivity observed in MTP-DAMA. cMPTP-DAMA, synthesized via direct copolymerization, exhibited improved mechanical integrity and dimensional stability due to covalent integration of rigid and flexible segments, albeit with reduced ionic cluster continuity. These modifications offered a balance between conductivity and physical durability, positioning them as viable alternatives where structural robustness is critical. Such results are consistent with previous studies demonstrating that blending with microporous components or incorporating block/random copolymer designs can synergistically improve ion transport and fuel cell performance.[22,23]

The AEMWE performance of the MTP-DAMA membrane was benchmarked against two commercial membranes, FAA-3-50 and Pention, under identical operating conditions (Figure S8). Pention was selected as the primary reference because it has a similar IEC and a crosslinked structure, which is also found in the membranes developed in this study. Despite these comparable membrane properties, MTP-DAMA (3.24) still delivered a significantly higher current density than Pention. At 2.0 V, the current density of MTP-DAMA (3.24) reached 7.7 A cm^{-2}, compared to 6.5 A cm^{-2} for Pention.

Comparative AEMWE performance was analyzed with recently reported AEMs (Figure S9).[73-81] To further benchmark the developed membranes, their electrolysis performance was compared with recently reported high-performance AEMs for water electrolysis. Notably, even the lower IEC membrane developed in this study exhibited electrolysis performance comparable to or exceeding that of several high-performance AEMs reported in the literature with higher IEC values.[73–75] Furthermore, the developed membranes maintained substantially lower water uptake while delivering highly competitive electrolysis performance. These results suggest that the excellent AEMWE performance achieved in this work cannot be attributed solely to IEC, but also to the effective optimization of membrane morphology, water management, and ion-transport pathways through backbone isomer engineering.

These results highlight that the membranes designed in this study are well-suited for high-performance, cost-effective, and scalable AEMWE systems. Furthermore, their ability to maintain performance when combined with non-PGM catalysts represents a significant advancement for sustainable hydrogen production technologies.

To evaluate water-lean operation, LSV and EIS tests were conducted using pure water (Figure S10, S11). MTP-DAMA (3.24) delivered current densities of 0.78 A cm^{-2} (PGM anode) and 0.86 A cm^{-2} (non-PGM anode), along with the lowest ohmic resistances (0.16 Ω cm^2 and 0.35 Ω cm^2, respectively).

The direct correlation between membrane hydration and current density was evident. Higher hydration facilitated the formation of continuous water channels, which enhanced OH^- diffusivity and reduced ohmic losses.

These results clearly demonstrate that water uptake, free volume, and ionic network connectivity jointly govern AEMWE performance.[18] Membranes with higher water content enabled more efficient ion transport, reduced ohmic resistance, and improved mass transfer, which translated to higher current densities during cell operation. This trend aligns well with the EIS analysis, where membranes with greater hydration exhibited lower ohmic and charge-transfer resistance. In line with this, Hu et al. reported reported similar results through a spirobisindane (SBI)-incorporated poly(aryl-co-aryl piperidinium) anion exchange membrane.[82] The twisted and rigid SBI core enlarged the free volume and facilitated continuous hydration pathways, which resulted in remarkably low RΩ and Rct values. Consequently, the membrane achieved a record current density o f 13.39 A cm^{-2} at 1.8 V.

Long-term AEMWE durability tests were commonly conducted under constant current conditions.[15] The MTP-DAMA membrane (IEC 1.97) was tested at 0.5 A cm^{-2} in 1 M KOH at 60 °C for 100 h using non-PGM anode catalyst for durability test (Figure 9a). The test was primarily designed to evaluate initial performance degradation and behavioral changes. The voltage rose modestly from 1.58 V to 1.72 V, indicating a degradation rate of ~1.3 mV h^{-1}. The post-test polarization curve showed a minor decline (~0.15 A cm^{-2} at 2.0 V), with negligible mass transport limitations. This suggests that degradation was predominantly due to slight bulk resistance accumulation, not interfacial delamination. The voltage loss at the operating current was limited to 0.13 V (Figure 9b), supporting the membrane's mechanical robustness and electrochemical durability. In this study, the system exhibited stable performance over 100 h, indicating sufficient durability. Therefore, extended testing beyond 100 hours was deemed unnecessary from both a scientific and resource-efficiency standpoint. In contrast, the ex-situ stability test aimed to assess the long-term chemical stability of the material under external environmental conditions, which justified the longer testing duration of 500 h.

From the perspective of long-term stability, PTP-based membranes demonstrated superior alkaline resistance, likely due to their dense morphology that hinders OH^- penetration. This trade-off highlights the need to balance conductivity and chemical robustness, particularly for prolonged operation in harsh alkaline environments.

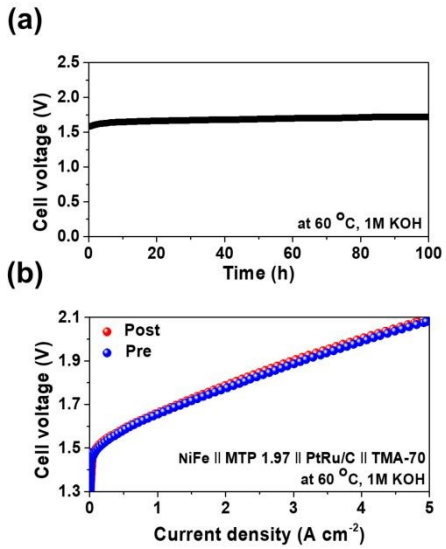

Figure 8. (a) Durability of MTP-DAMA (1.97) under 0.5 A cm^{-2} constant current conditions (b) LSV curves before and after durability tests

Conclusions

In this work, we developed a series of pyrrolidinium-based anion exchange membranes (AEMs) incorporating m- and p-terphenyl backbones to investigate the role of isomeric geometry and polymer integration strategy in tuning membrane performance. Through systematic comparison of homopolymers, physical blends, and random copolymers, we demonstrated how polymer backbone conformation and macromolecular architecture govern key properties such as free volume, hydration behavior, hydroxide conductivity, and mechanical robustness.

Membranes containing twisted MTP units exhibited increased free volume and enhanced water uptake, leading to higher ionic conductivity. In contrast, linear PTP structures conferred superior mechanical strength and dimensional stability. Physical blending of the two backbones enabled enhanced ionic transport through heterogeneous phase formation, while covalent copolymerization led to improved chemical durability and uniform morphology. Notably, MTP-DAMA membranes achieved a rare combination of high conductivity, low ohmic resistance, and long-term stability under both KOH and pure water conditions. In addition, they outperformed commercial membranes such as FAA-3 even when operated with a non-PGM anode.

These results establish that both backbone isomerism and integration method are critical design parameters for balancing transport efficiency and structural stability. The complementary performance of bMPTP-DAMA and cMPTP-DAMA further supports the utility of blending and copolymerization strategies in optimizing AEM properties for practical applications.

Our findings provide molecular-level insights into the structure–property–performance relationships of AEMs and highlight isomeric backbone engineering as a general and scalable strategy for the design of high-performance, durable membranes. This approach holds promise not only for AEMWE but also for broader alkaline electrochemical applications, including fuel cells and CO_2 reduction. Future efforts may explore block copolymer designs, controlled nanoscale phase separation, or alternative isomer configurations to further advance membrane functionality.

Author contributions

Dana Kim: conceptualization, validation, formal analysis, writing-original draft. Jeongmin Jang: formal analysis, investigation. Jiyoon Jung: formal analysis, Jinsuk Ku: formal analysis, Young Sang Park: formal analysis, data curation. Jung-Hyun Lee: writing-review and editing, supervision. Albert S. Lee: validation, formal analysis, writing-original draft, writing-review and editing, supervision.

Conflicts of interest

The authors declare that they have no known competing financial interests or personal relationships that could have appeared to influence the work reported in this paper.

Data availability

Data will be made available on request.

Acknowledgements

A. S. Lee acknowledges support by the Nano & Material Technology Development Program through the National Research Foundation of Korea (NRF) funded by Ministry of Science and ICT (RS-2024-00450102) with 50 % contribution, the National Research Council of Science & Technology (NST) grant by the Korea government (MSIT) (CRC22031-000) the institutional program at KIST (2V10154), and the National Research Foundation of Korea(NRF) grant funded by the Korea government (MSIT) (RS-2025-16072584).

Notes and references

1 S. S. Kumar and H. Lim, *Energy Rep.*, 2022, **8**, 13793 – 13813.
2 Y. Yang, C. R. Peltier, R. Zeng, R. Schimmenti, Q. Li, X. Huang, Z. Yan, G. Potsi, R. Selhorst, X. Lu, W. Xu, M. Tader, A.V. Soudackov, H. Zhang, M. Krumov, E. Murray, P. Xu, J. Hitt, L. Xu, H. Y. Ko, B.G. Ernst, C. Bundschu, A. Luo, D. Markovich, M. Hu, C. He, H. Wang, J. Fang, R.A. DiStasio Jr., L. F. Kourkoutis, A. Singer, K. J. T. Noonan, L. Xiao, L. Zhuang, B. S. Pivovar, P. Zelenay, E. Herrero, J. M. Feliu, J. Suntivich, E. P. Giannelis, S. Hammes-Schiffer, T. Arias, M. Mavrikakis, T. E. Mallouk, J. D. Brock, D. A. Muller, F. J. DiSalvo, G. W. Coates and H. D. Abruna, *Chem. Rev.*, 2022, **122**, 6117 – 6321.
3 C. Li and J. B. Baek, *Nano Energy*, 2021, **87**, 106162.
4 N. Du, C. Roy, R. Peach, M. Turnbull, S. Thiele and C. Bock, *Chem. Rev.*, 2022, **122**, 11830 – 11895.

5 D. Henkensmeier, M. Najibah, C. Harms, J. Žitka, J. Hnát and K. Bouzek, *J. Electrochem. Energy Convers. Storage*, 2021, **18**, 024001.
6 B. C. Bae, E. Y. Kim, S. J. Lee and H. J. Lee, *New. Renew. Energy*, 2015, **11**, 52 – 61.
7 Z. Jiang, G. Yi, X. Yao, Y. Ma, X. Su, Q. Liu and Q. Zhang, *Chem. Eng. J.*, 2023, **467**, 143442.
8 R. Espiritu, B. T. Golding, K. Scotta and M. Mamlouk, *J. Mater. Chem. A*, 2017, **5**, 1248 – 1267.
9 J. R. Varcoe, P. Atanassov, D. R. Dekel, A. M. Herring, M. A. Hickner, P. A. Kohl, A. R. Kucernak, W. E. Mustain, K. Nijmeijer, K. Scott, T. Xuk and L. Zhuang, *Energy Environ. Sci.*, 2014, **7**, 3135 – 319.
10 A. Raut, H. Fang, Y. C. Lin, D. Sprouster, Y. Yin, Y. Fang, S. Fu, S. Sharma, L. Wang, C. S. Bae and M. Rafailovich, *Energy Adv.*, 2023, **2**, 113 – 122.
11 P. P. Kundu and R. C. Larock, *Biomacromolecules*, 2005, **6**, 797 – 806.
12 C. Fujimoto, D. S. Kim, M. Hibbs, D. Wrobleski and Y. S. Kim, *J. Membr. Sci.*, 2012, **423–424**, 438 – 449.
13 M.G. Marino and K. D. Kreuer, *ChemSusChem*, 2015, **8**, 513 – 523.
14 D. L. Safranski and K. Gall, *Polymer*, 2008, **49**, 4446 – 4455.
15 C. Hu, Y. Wang and Y. M. Lee, *Angew. Chem. Int. Ed.*, 2025, **64**, e202418324.
16 Z. Xu, S. Delgado, V. Atanasov, T. Morawietz, A. S. Gago and K. A. Friedrich, *Membranes*, 2023, **13**, 328.
17 S. Gjoshi, P. Loukopoulou, M. Plevova, J. Hnat, K. Bouzek and V. Deimede, *Polymers*, 2024, **16,** 99.
18 J. Xue, J. C. Douglin, T. Huang, H. Jiang, J. Zhang, Y. Yin, D. R. Dekel and M. D. Guiver, *J. Membr. Sci.*, 2025, **717**, 123519.
19 W. H. Lee, E. J. Park, J. Y. Han, D. W. Shin, Y. S. Kim and C. S. Bae, *ACS Macro Lett.*, 2017, **6**, 566 – 570.
20 W. Gao, X. Gao, Q. Zhang, A. Zhu and Q. Liu, *J. Energy Chem.*, 2024, **89**, 324 – 335.
21 P. M. Bakvand, D. Pan, A. Allushi and P. Jannasch, *Adv. Energy Mater.*, 2024, **15**, 2402869.
22 S. Gong, L. Li, L. Ma, N. A. Qaisrani, J. Liu, G. He and F. Zhang, *J. Membr. Sci.*, 2020, **595**, 117541.
23 M. Mandal, G. Huang, N. U. Hassan, W. E. Mustain and P. A. Kohl, *J. Mater. Chem. A*, 2020, **8**, 17568 – 17578.
24 G. B. Butler and A. Crawshaw, W. L. Miller, *J. Am. Chem. Soc.*, 1958, **80**, 3615 – 3618.
25 M. T. Guzmán-Gutiérrez, D. R. Nieto, S. Fomine, S. L. Morales, M. G. Zolotukhin, M. C. G. Hernandez, H. Kricheldorf and E. S. Wilks, *Macromolecules*, 2011, **44**, 194 – 202.
26 S. V. Pronin, C. A. Reiher and R. A. Shenvi, *Nature*, 2013, **501**, 195 – 199.
27 W. M. Lee, *Polym. Eng. Sci.*, 1980, **20**, 65-69.
28 S. X. Cheng, T. S. Chung, R. Wang and R. H. Vora, *J. Appl. Polym. Sci.*, 2003, **90**, 2187 – 2193.
29 S. H. Kwon, A. H. N. Rao and T. H. Kim, *J. Power Sources*, 2018, **375**, 421 – 432.
30 Z. Wang, G. Sun, N. H. C. Lewis, M. Mandal, A. Sharma, M. C. Kim, J. M. M. Oca, K. Wang A. Taggart, A. B. Martinson, P. A. Kohl, A. Tokmakoff, S. N. Patel, P. F. Nealey and J. J. Pablo, *Nat. Commun.*, 2025, **16**, 1099.
31 R. Kingsbury, M. Hegde, J. Wang, A. Kusoglu, W. You and O. Coronell, *ACS Appl. Mater. Interfaces*, 2021, **13**, 52647 – 52658.
32 G. H. Choi, M. G. Nam, S. J. Kwak, S. H. Kim, H. Chang, C. S. Shin, W. B. Lee and P. J. Yoo, *Energy Environ. Sci.*, 2019, **14**, 3203 – 3215.
33 D. G. Li, E. J. Park, W. Zhu, Q. Shi, Y. Zhou, H. Tian, Y. Lin, A. Serov, B. Zulevi, E. D. Baca, C. Fujimoto, H. T. Chung and Y. S. Kim, *Nat. Energy*, 2020, **5**, 378 – 385.
34 P. J. Flory, *J. Am. Chem. Soc.*, 1945, **67**, 2048 – 2050.
35 A. Oxley and A. G. Livingston, *J. Membr. Sci.*, 2024, **689**, 122149.
36 W. K. Ng, W. Y. Wong, N. A. H. Rosli and K. S. Loh, *Separations*, 2023, **10**, 424.
37 Y. J. Kim, Y. S. Park, S. G. Han, W. C. Park, M. G. Kim, K. H. Kim, J. M. Joo, S. K. Hahn and W. S. Kwon, *Nanomaterials*, 2022, **12**, 70.
38 D. P. Dowling, C. E. Nwankire, M. Riihimäki, R. Keiski and U. Nylé, *Surf. Coat. Tech.*, 2010, **205**, 1544 – 1551.
39 W. Zhang, W. Cheng, R. A. Tufa, C. Liu, D. Aili, D. Chanda, J. Chang, S. Wang, Y. Zhang and J. Ma, *Membranes*, 2021, **11**, 771.
40 T. Hamada, T. Sugimoto, A. Tanaka, T. Maeda, D. Katsura, H. Koga and J. Ohshita, *RSC Appl. Polym.*, 2025, **3**, 92 – 96.
41 K. Goto, I. Rozhanskii, Y. Yamakawa, T. Otsuki and Y. Naito, *Polym. J.*, 2009, **41**, 95 – 104.
42 Y. Yagizatli, A. Sahin and I. Ar, *Int. J. Hydrogen Energy*, 2022, **47**, 40445 – 40461.
43 K. Mazumder, H. Nederstedt, R. Weber, S. Haraguchi, R. Neubert, F. A. Plamper, C. Müller and M. Sommer, *ACS Appl. Mater. Interfaces*, 2025, **17**, 41978 – 41990.
44 R. Winkler, K. Chat, A. B. Unni, M. Dulski, M. Laskowska, L. Laskowski and K. Adrjanowicz, *Macromolecules*, 2022, **55**, 3208 – 3220.
45 J. C. Lee and M. H. Litt, *Polym. J.*, 2000, **32**, 228 – 233.
46 A. M. Spring, D. Maeda, M. Ozawa, K. Odoi, F. Qiu, K. Yamamoto and S. Yokoyama, *Polymer Bull.*, 2015, **72**, 503 – 521.
47 O. Racchi, R. Baldassari, E. A. Hermosilla, V. Mattoli, P. Minei, A. Pozio and A. Pucci, *Polymers*, 2023, **15**, 2027.
48 H. Khalid, M. Najibah, H. S. Park and C. S. Bae, *Membranes*, 2022, **12**, 989.
49 W. Song, K. Peng, W. Xu, X. Liu, H. Zhang, X. Liang, B. Ye, H. Zhang, Z. Yang, L. Wu, X. Ge and T. Xu, *Nat. Commun.*, 2023, **14**, 2732.
50 Y. U. Kim, B. S. Ma, Y. N. Kim, S. H. Park, H. G. Kang, H. J. Yoon, M. J. Cho, T. S. Kim, J. H. Kim and D. H. Choi, *Chem. Eng. J.*, 2021, **415**, 128952.
51 G. Huang, M. Mandal, N. U. Hassan, K. Groenhout, A. Dobbs, W. E. Mustain and P. A. Kohl, *J. Electrochem. Soc.*, 2020, **167**, 164514.
52 S. Zhang, W. Ma, L. Tian, D. Kong, Q. Zhu, F. Wang and H. Zhu, *ACS Appl. Mater. Interfaces*,2024, **16**, 7660 – 7669.
53 C. He, J. Liu, J. Li, F. Zhu and H. Zhao, *J. Membr. Sci.*, 2018, **560**, 30 – 37.
54 L. Tao, J. He, T. Arbaugh, J. R. McCutcheon and Y. Li, *J. Membr. Sci.*, 2023, **665**, 121131.
55 A. X. Wu, S. Lin, K. M. Rodriguez, F. M. Benedetti, T. Joo, A. F. Grosz, K. R. Storme, N. Roy, D. Syar and Z. P. Smith, *J. Membr. Sci.*, 2021, **636**, 119526.
56 Z. Yang, R. Guo, R. M. Evans, M. Carta, N. B. McKeown, M. D. Guiver, L. Wu and T. Xu, *Angew. Chem. Int. Ed.*, 2016, **55**, 11499.
57 C. Yuan, Y. Chen, X. Lu, X. Ma, W. Yuan, X. Zhu, B. Chen, J. Wang and Z. Wei, *J. Membr. Sci.*, 2024, **701**, 122769.
58 T. Hatakeyama, K. Nakamura and H. Hatakeyama, *Thermochim. Acta*, 1988, **123**, 153 – 161.
59 S. P. Tung and B. J. Hwang, *J. Membr. Sci.*, 2004, **241**, 315 – 323.
60 D. Capitani, V. Crescenzi, A. A. De Angelis and A. L. Segre, *Macromolecules*, 2001, **34**, 4136 – 4144.
61 B. E. Kinn, T. R. Myers and A. M. Allgeier, *Curr. Opin. Chem. Eng.*, 2019, **24**, 115 – 121.
62 L. Li, X. Xu, L. Liu, P. Song, Q. Cao, Z. Xu, Z. Fang and H. Wang, *Polymer*, 2021, **213**, 123330.
63 X. Wu, N. Chen, H. A. Klok and Y. M. Lee, *Angew. Chem. Int. Ed.*, 2022, **61**, e202114892.

View Article Online
DOI: 10.1039/D6TA02924H

64 G. H. A. Wijaya, K. S. Im and S. Y. Nam, *Desalin. Water Treat.*, 2024, **320**, 100605.
65 A. Zhegur, N. Gjineci, S. W. Cohen, A. N. Mondal, C. E. Diesendruck, N. Gavish and D. R. Dekel, *ACS Appl. Polym. Mater.*, 2020, **2**, 360 – 367.
66 P. M. Mangiagli, C. S. Ewing, K. Xu, Q. Wang and M. A. Hickner, *Fuel Cells*, 2009, **9**, 432 – 438.
67 W. E. Mustain, M. Chatenet, M. Pagec and Y. S. Kim, *Energy Environ. Sci.*, 2020, **13**, 2805 – 2838.
68 M. I. Khan, X. Li, J. F. Garcia, M. H. Lashari, A. U. Rehman, N. Elboughdiri, L. Kolsi and D. Ghernaout, *ACS Omega*, 2021, **6**, 7994 – 8001.
69 L. Wang, X. Peng, W. E. Mustain and J. R. Varcoe, *Energy Environ. Sci.*, 2019, **12**, 1575 – 1579.
70 J. E. Park, S. Y. Kang, S. H. Oh, J. K. Kim, M. S. Lim, C. Y. Ahn, Y. H. Cho and Y. E. Sung, *Electrochim. Acta*, 2019, **295**, 99 – 106.
71 S. Siracusano, V. Baglio, N. Van Dijk, L. Merlo and A. S. Aricò, *Appl. Energy*, 2017, **192**, 477 – 489.
72 A. W. Tricker, T. Y. Ertugrul, J. K. Lee, J. R. Shin, W. Choi, D. I. Kushner, G. Wang, J. Lang, I. V. Zenyuk, A. Z. Weber and X. Peng, *Adv. Energy Mater.*, 2023, **14**, 2303629.
73 Z. Peng, R. Zhang, W. Zhao, Y. WU, Y. Zhao and J. Yang, *J. Membr. Sci.*, 2026, **738**, 124827.
74 Q. Wang, T. Wei, Z. Peng, Y. Zhao, P. Jannasch and J. Yang, *J. Colloid Interface Sci.*, 2025, **686**, 304-317.
75 Z. Peng, Z. Ren, S. Chen, Y. Zhao, P. Jannasch and J. Yang, *Int. J. Hydrogen Energy*, 2025, **188**, 151884
76 S. Jeon, H. W. Kang, K. Min, W. Lee, H. Maeng, C. H. Park and T. H. Kim, *J. Membr. Sci.*, 2025, **726**, 124050.
77 Z. Peng, T. Wei, Q. Wang, Y. Zhao and J. Yang, *J. Power Sources*, 2025, **642**, 236918.
78 W. Zou, G. Tang, K. Peng, X. Mo, T. Hu, Z. Yang and T. Xu, *Angew. Chem. Int. Ed.*, 2025, **137**, e202514264.
79 T. He, R. Shen, C. Lin, A. Zhu, Z. Xie and Q. Zhang, *J. Membr. Sci.*, 2025, **728**, 124148.
80 W. Zheng, L. He, T. Tang, R. Ren, H. Lee, G. Ding, L. Wang and L. Sun, *Angew. Chem. Int. Ed.*, 2024, **136**, e202405738.
81 T. Tang, H. Lee, Z. Wang, Z. Li, L. Wang, D. Chen, W. Zheng, Q. Liu, L. He, G. Ding, Z. Tian and L. Sun, *Energy Environ. Sci.*, 2024, **17**, 7816–7828.
82 C. Hu, H. W. Kang, S. W. Jung, M. L. Liu, Y. J. Lee, J. H. Park, N. Y. Kang, M. G. Kim, S. J. Yoo, C. H. Park and Y. M. Lee, *Adv. Sci.*, 2023, **11**, 2306988.

View Article Online
DOI: 10.1039/D6TA02924H

Data Availability Statement

Data will be available upon reasonable request.